Please cite this article in press as: Strimbu et al., Manipulation of the Endocochlear Potential Reveals Two Distinct Types of Cochlear Nonlinearity, Biophysical Journal (2020), https://doi.org/10.1016/j.bpj.2020.10.005

Biophysical *Journal*
Article

Biophysical Society

Manipulation of the Endocochlear Potential Reveals Two Distinct Types of Cochlear Nonlinearity

C. Elliott Strimbu,[1] Yi Wang,[2] and Elizabeth S. Olson[1,2,*]
[1]Columbia University Medical Center, Department of Otolaryngology, New York, New York and [2]Columbia University, Department of Biomedical Engineering, New York, New York

ABSTRACT The mammalian hearing organ, the cochlea, contains an active amplifier to boost the vibrational response to low level sounds. Hallmarks of this active process are sharp location-dependent frequency tuning and compressive nonlinearity over a wide stimulus range. The amplifier relies on outer hair cell (OHC)-generated forces driven in part by the endocochlear potential, the ~+80 mV potential maintained in scala media, generated by the stria vascularis. We transiently eliminated the endocochlear potential in vivo by an intravenous injection of furosemide and measured the vibrations of different layers in the cochlea's organ of Corti using optical coherence tomography. Distortion product otoacoustic emissions were also monitored. After furosemide injection, the vibrations of the basilar membrane lost the best frequency (BF) peak and showed broad tuning similar to a passive cochlea. The intra-organ of Corti vibrations measured in the region of the OHCs lost the BF peak and showed low-pass responses but retained nonlinearity. This strongly suggests that OHC electromotility was operating and being driven by nonlinear OHC current. Thus, although electromotility is presumably necessary to produce a healthy BF peak, the mere presence of electromotility is not sufficient. The BF peak recovered nearly fully within 2 h, along with the recovery of odd-order distortion product otoacoustic emissions. The recovery pattern suggests that physical shifts in operating condition are a critical step in the recovery process.

SIGNIFICANCE Intracochlear vibrations are boosted by an active, nonlinear feedback process that endows the cochlea with its sensitivity and frequency tuning. Tuned responses derive from outer hair cell (OHC) electromechanical forces, driven by OHC transducer current. A standing potential across the cochlear partition is necessary for normal operation. We transiently eliminated this potential and monitored the effect on cochlear mechanics. Nonlinearity in vibration responses, evincing OHC electromechanics, dropped but could recover within an hour, whereas frequency tuning was eliminated and recovered over 2 h. Odd-order distortion, signaling physical centering of the OHC transducer nonlinearity, recovered over the slower time frame. Thus, OHC electromechanics are not sufficient for the recovery of cochlear frequency tuning; physical operating conditions are also critical.

INTRODUCTION

In the mammalian cochlea, the sound signal, in the form of traveling pressure and motion waves, is converted to electrical signals by the sensory hair cells that lie within the organ of Corti (Fig. 1). Arrays of tightly packed stereocilia (hair bundles) of graded height protrude from the apical surface of the hair cells. During hearing, relative motion between the tectorial membrane, an acellular structure that overlies and couples the hair cells, and the reticular lamina located at the apical surface of the hair cell bodies, results in pivoting of the hair bundles. When the stereocilia deflect toward/away from their tallest row, mechanically gated ion channels on the shorter rows are opened/closed, and the flow of cations, mostly K^+ (also Ca^{2+}), is increased/reduced and depolarizes/hyperpolarizes the hair cells. Complex sounds are resolved into frequency components that peak at different locations along the length of the cochlea with high frequencies encoded at the base and low frequencies encoded at the apex.

The mechanical vibrations of the organ of Corti complex (OCC) (organ of Corti (OC), tectorial membrane (TM), and basilar membrane (BM)) are boosted by the cochlear amplifier, an active process or set of coupled processes operating under feedback. A key component of amplification is generated by the outer hair cells (OHCs); in response to changes in the membrane potential, the OHC soma changes length in a process driven by the motor protein prestin (1). The

Submitted May 13, 2020, and accepted for publication October 7, 2020.
*Correspondence: eao2004@columbia.edu
Editor: Jeremiah Zartman.
https://doi.org/10.1016/j.bpj.2020.10.005

Please cite this article in press as: Strimbu et al., Manipulation of the Endocochlear Potential Reveals Two Distinct Types of Cochlear Nonlinearity, Biophysical Journal (2020), https://doi.org/10.1016/j.bpj.2020.10.005

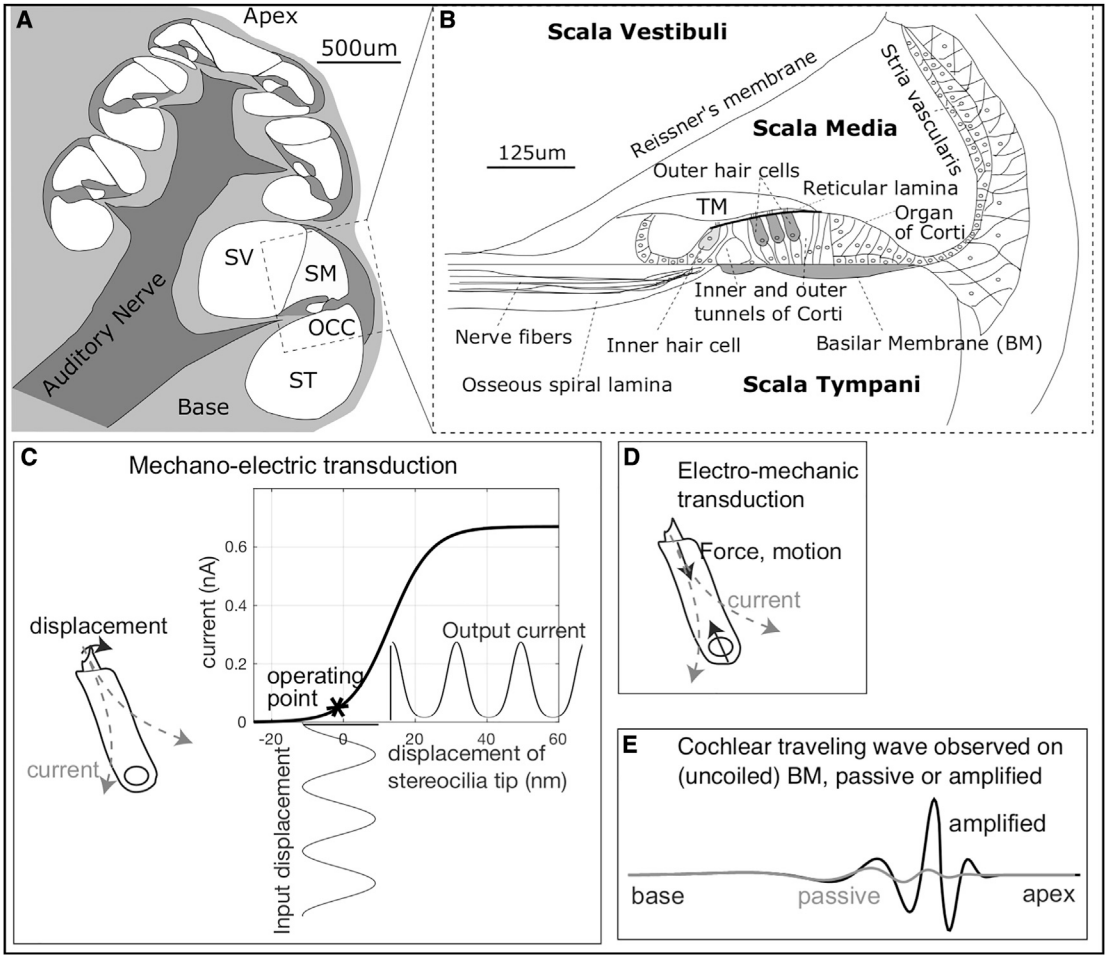

FIGURE 1 (*A*) Cross-sectional sketch of the gerbil cochlea, with fluid compartments scala media (SM), scala tympani (ST), and scala vestibuli (SV) labeled. (*B*) The boxed section in (*A*) is expanded, to show the organ of Corti complex (OCC). The OCC is composed of the sensory tissue of the organ of Corti (including the inner and outer hair cells (OHC)) and surrounding acellular structures of the basilar membrane (BM) and tectorial membrane (TM). (*C*) Nonlinearity is based in the saturation of OHC current when MET channels are pushed to the nearly fully open and fully closed states. OHC current data and Boltzmann input-output function were redrawn from (6). The "operating point" (OP) is the position on the input/output curve that the input sinusoid is centered on and is noted by an asterisk. (*D*) The mechanical basis of amplification—defined as the enhanced tuning and sensitivity of a healthy cochlea—is most likely OHC somatic forces arising from the prestin molecule's conformation changes after electromechanic transduction. (*E*) Cartoon of the motion response to a tone on the BM shows the characteristic amplification in the region where the responses peak and illustrating that amplification will make otherwise undetectable signals large enough to be detectable and enhance frequency resolution.

cochlear amplifier increases the response to low level sounds, resulting in a compressive nonlinearity that boosts the dynamic range of hearing across some six orders of stimulus pressure magnitude (2–4). In healthy cochleae, the vibrations at low sound pressure levels (SPLs) are sharply peaked at each longitudinal location's best frequency (BF) (Fig. 1 *E*). Thus, the cochlear amplifier increases both sensitivity and frequency resolution. In cochleae for which the active process is not functional, for example, post mortem, and after damage, the responses become linear and exhibit broad tuning. Broad tuning is also typically observed at stimulus levels greater than ∼80 dB SPL (defined as dB relative to 20 μPa). OHC electromotility is most likely responsible for amplifying the OCC vibrations, whereas the nonlinearity is due to saturation in mechanoelectric transduction (MET) (Fig. 1, *C* and *D*; (5,6)). The nonlinearity of the cochlear amplifier produces distortion product otoacoustic emissions (DPOAEs). When two or more tones are presented simultaneously, additional frequencies are generated in the cochlea and reverse propagate to the middle ear. The resulting motion of the eardrum then produces faint sounds at these distortion frequencies that can be measured in the ear canal. DPOAEs are a noninvasive gauge of cochlear condition and have also been used to detect operating point (OP) shifts in the MET nonlinearity (Fig. 1 *C*; (7,8)).

The MET currents are driven in part by the endocochlear potential (EP), the ∼+80 mV electrical potential within the scala media. The EP is generated by cells within the stria vascularis (Fig. 1 *B*). Gradual degradation of the stria

Please cite this article in press as: Strimbu et al., Manipulation of the Endocochlear Potential Reveals Two Distinct Types of Cochlear Nonlinearity, Biophysical Journal (2020), https://doi.org/10.1016/j.bpj.2020.10.005

vascularis and the corresponding decline in the EP is one cause of presbyacusis, or age-related hearing loss, which affects up to half of the population over 75 years of age in the United States (9–11). Loop diuretics such as furosemide cause a sudden and reversible decrease in the EP and have been used in vivo in animal studies to investigate the effects of EP reduction on mechanical (12) and electrical (13–16) responses within the cochlea and on DPOAEs (16–18).

In recent studies by our group (16), furosemide was administered intravenously (iv) to gerbil, and EP was monitored continuously along with the extracellular voltage measured close to the BM. We termed this voltage "local cochlear microphonic" (LCM). The LCM shows tuning and traveling wave phase excursion similar to the motion of the adjacent OCC and is useful for exploring cochlear amplification (19–21). LCM is a measure of OHC current (22), and its saturation can be used as an in vivo probe of saturation and OP shifts in MET (Fig. 1 *C*; (7,16,21)). In the furosemide plus LCM experiments, after a deep reduction in EP and LCM responses, both recovered but with different timescales. EP recovered and stabilized at a subnormal voltage by ∼40 min (Fig. 2 *A*). (EP was not measured in the current study for practical reasons, and we assume that a similar time course holds in the current study, which used an identical iv furosemide protocol.) Others have also observed a rapid initial recovery followed by a plateau after iv furosemide (13,14). In our recent study, the LCM BF peak recovered more slowly than EP, with a burst of recovery at ∼60 min that could lead to full recovery of the LCM BF peak at 100 min. Two of these LCM results will be shown with OCC displacement data in Fig. 5. As the LCM peak recovered, LCM second harmonics diminished, and third harmonics and $2f_1–f_2$ distortion products increased. Interpreted in the framework of a Boltzmann input-output function, this pattern of recovery (odd-order distortion increasing and even-order distortion decreasing) signaled that the OP on the Boltzmann function was centering during recovery (7,16,23). As noted above, the site of nonlinearity is thought to be the hair cell MET channel (5,6). The OP shift was analyzed in quantitative detail in one experiment and is shown in Fig. 2 *B* with the *y* axis both in Pascals and converted to estimated stereocilia pivoting using results from the literature (6). As a further background note on the OP of the cochlear nonlinearity, in healthy cochleae, the OP is not exactly centered as evinced in even-order distortion products and summating potential (23–25).

The finding that LCM BF peak recovery lags EP recovery and coincides with an OP shift in MET posed questions: What is happening during the recovery process after EP is stable? Perhaps OHCs detached from the TM after furosemide and reattach during recovery to resume OHC electromotile forcing. Such a proposal is reasonable; detachment/reattachment occurs after noise exposure (26). Perhaps OHC stereocilia have been damaged by the reduction in

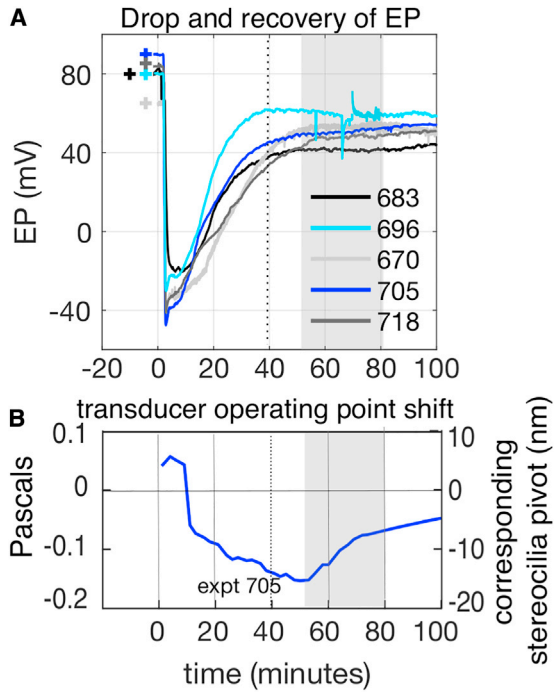

FIGURE 2 Furosemide-induced EP and MET OP shift observed in a precursor study that followed the same iv furosemide protocol as this study (16). (*A*) After iv furosemide, EP dropped immediately to −20 to −40 mV, began recovering within 10 min, and stabilized at a subnormal level ∼40 min after furosemide delivery (*vertical dotted line*). (*B*) MET OP shift was measured with fine time resolution in one experiment (refer to Fig. 1 *C*). Left axis shows OP in terms of stimulus pressure, and right axis shows OP in terms of stereocilia bundle resting point. After furosemide, the OP started positive, shifted negative to its least-centered value at ∼50 min, and then returned toward zero with the largest increase from 50 to 80 min. This time frame coincided with the recovery of the compressively nonlinear BF peak (16). The timing of the EP recovery and OP variations are useful background information for analyzing the results of this study. To see this figure in color, go online.

MET current during the brief time when EP became negative and are recovering over 1–2 h (27). More generally, what is the constellation of factors that must align to produce the remarkable sensitivity and frequency resolution of the cochlea?

To explore these proposed mechanisms and pursue the overarching question, in this study, we used phase sensitive spectral domain (SD) optical coherence tomography (OCT) (28) to measure the sound-induced vibrations within the OCC in vivo before and after the EP was perturbed by an iv injection of furosemide. SD-OCT makes simultaneous measurements at multiple locations along the axis of the OCT beam, enabling simultaneous recording from different layers within the organ of Corti. DPOAEs were also monitored. To give a brief preview of findings, after furosemide, BM vibrations lost the compressively nonlinear BF peak and became nearly passive, similar to findings in previous studies (12). The vibrations in the OHC region lost the BF peak and became low pass but retained wideband compressive nonlinearity. This wideband nonlinearity is taken to be

Please cite this article in press as: Strimbu et al., Manipulation of the Endocochlear Potential Reveals Two Distinct Types of Cochlear Nonlinearity, Biophysical Journal (2020), https://doi.org/10.1016/j.bpj.2020.10.005

an expression of OHC electromotility, an expectation that is supported by the observation that the LCM, representing OHC current, shows substantial wideband nonlinearity when elicited with the multitone stimuli used in this report (21). The compressively nonlinear BF displacement peak in both BM and OHC started to emerge at ~50 min and could recover nearly completely by 120 min. The $2f_1$–f_2 DPOAE from the BF region recovered nonmonotonically, dipping to a local minimum at ~50 min followed by a burst of recovery from 50 to 100 min to its pre-furosemide level. The similar time course of BF peak and odd-order distortion recovery is in line with the observation from the LCM study that recovery of the BF peak was linked to recentering of the MET channel OP. The persistence of wideband nonlinear displacement at sub-BF frequencies indicates that electromotility remained robust throughout and sheds light on the possibilities for the recovery process and the factors required for amplification of the BF peak.

MATERIALS AND METHODS

Gerbil preparation

The experiments were approved by the Columbia University Institutional Animal Care and Use Committee. Young adult gerbils, ~7–11 weeks old, of either sex were anesthetized with intraperitoneal injections of ketamine (40 mg/kg) and sodium pentobarbital (40 mg/kg). Anesthesia was maintained with supplemental doses of pentobarbital given if the animals displayed a reflex in response to a light toe pinch. Buprenorphone (0.2 mg/kg) was administered intraperitoneal every 6 h. The gerbil's scalp was removed, and the head attached to a two-axis goniometer (Melles-Griot, Carlsbad, CA) with dental cement (Durelon, Philadelphia, PA; 3M). The left pinna and most of the cartilaginous ear canal were resected, and the animals were tracheotomized to facilitate breathing. The tissue and muscle over the left temporal bone were carefully dissected, and a narrow opening in the bulla was made by chipping the bone with fine forceps. A bridge of dental cement was used to firmly attach the bulla to the goniometer. Throughout the surgery and experiment, the animal's temperature was maintained at 38°C with a servocontrolled heating blanket and monitored with a rectal thermometer. During the OCT measurements, additional heating to the animal's head was supplied by a disposable hand warmer (Hot Hands; HeatMax, Dalton, GA) positioned on the goniometer. Experiments were conducted on an optics table in an acoustical isolation booth (Industrial Acoustics, Bronx, NY).

Acoustical system

Acoustic signals were generated using a Tucker Davis Technologies (TDT) system with a sampling rate of 97,656.25 S/s. The sound was played by a RadioShack (Fort Worth, TX) speaker and delivered closed-field to the ear canal through a plastic tube. Pressures were measured with an ultrasonic microphone (Sokolich) whose probe tube was positioned 1–2 mm from the tympanic membrane. Sound pressure levels are reported as dB SPL referenced to the standard value, 0 dB = 20 μPa. The OCT and TDT systems were synchronized as previously described (28). The clock signal from the TDT zBus was modified using a custom-built digital/analog circuit to give a high duty cycle (90% high, 10% low) 5 V square wave, which served as the trigger for the OCT's line camera. Tuning curves were measured in response to zwuis tone complexes (29,30); 60 frequencies from ~4 to ~37 kHz were presented simultaneously for $2^{20} = 1048576$ shots or 10.7 s at 40–80 dB SPL in 10 dB steps. The frequencies were chosen such that each component contained an integer number of points per cycle, and the stimulus contained no harmonics or distortion products up to third order (30). Each sinusoidal component in the complex was assigned a random phase so the pressure magnitude of the complex was $\sim\sqrt{60}$ higher than the magnitude of each component. DPOAEs in response to swept two-tone (f_1 and f_2) stimuli were measured before each set of tuning curves throughout the experiment. In these measurements, f_2 was varied from 1 to 48 kHz, f_1 and f_2 were held at a fixed ratio of $f_2 = 1.2\,f_1$, and the two primary tones were presented at 50 and 70 dB SPL. The stimulus repeated seamlessly 50 times, for a total time of ~1 s, and the 50 time-locked responses were averaged. The noise level was typically −3 to 0 dB SPL for the DPOAE recordings.

OCT and SD phase microscopy

Cochleae were imaged with a ThorLabs Telesto III OCT equipped with an LSM03 5×, 0.055 NA objective lens. After the initial surgery, the gerbils were placed under the OCT, and the instrument's video camera and an operating microscope were used to position the head. Recordings were made in the cochlear base near the 25 kHz location, found by aiming the system apically through the round window. Initially, continuous two-dimensional scanning was done with the ThorImage program and small adjustments made to the position until the OCC was centered in the field of view. The position was adjusted until the two gaps in the organ of Corti corresponding to the inner and outer tunnels (Fig. 1 *B*) were visible in the B- and A-scans (Fig. 3). For vibrometry, the OCT was controlled with custom software written in C++, based on the ThorLabs software development kit. Before and after each set of tuning curves, the OCT acquired 1-mm wide B-scans, and the two images were compared to confirm that the sample was stable over the course of the measurement.

For vibrometry, a single A-scan through the BM and OHC region was selected, and time-locked A-scan spectra were recorded as the sound played and then saved to a hard disk as 16-bit raw files for offline analysis. The time series of spectra (termed M-scan) were converted to a series of complex numbers representing reflectivity versus depth (see (28) for analytical details). Pixels of local maxima in the time-averaged A-scan magnitude, corresponding to specific features in the OCT image, were selected for further analysis, for example, a pixel on the round window membrane and several pixels in the BM and OHC region. In SD phase microscopy, the displacement versus time of each pixel in the A-scan is proportional to the phase versus time of the complex M-scan at that pixel. The noise level in the vibration measurement is determined by the magnitude of the selected A-scan pixel, which depends on the feature and reflectivity. In the best preparations, the noise floor could be as low as 0.02–0.05 nm. Noise rises if the A-scan peak is reduced (Fig. 3 *A* and *B*), which can happen because of micrometer-scale shifts in the preparation. Several baseline measurements were made before the furosemide to establish a solid baseline, and the most complete data set was used for presentation. The vibration and interleaved DPOAE measurements were stable during these baseline runs; the baseline DPOAE results in Fig. 6 indicate physiological stability.

Once the vibration time waveforms were acquired for the regions of interest, the amplitudes and phases at the sound stimulus frequencies were extracted by Fourier analysis. For each stimulus frequency, the response was deemed significant if the Fourier coefficient was 3.2 times larger than the SD of the noise level, measured from 10 neighboring bins in the spectra. In the presented plots, when individual data points met that criterion but neighboring points did not, they were usually removed; this removed distracting isolated points that were very close to the defined noise floor. The resulting tuning curves are presented in terms of the gain, defined as displacement per unit pressure. The phases are referenced to the ear canal pressure. Analysis scripts were custom written in MATLAB (The MathWorks, Natick, MA).

At the start of an experiment, we tested the displacements at one or more locations by playing a short zwuis complex containing 10 frequencies from 10 to 40 kHz at 60, 70, and 80 dB SPL for 1 s. We could perform a complete

Please cite this article in press as: Strimbu et al., Manipulation of the Endocochlear Potential Reveals Two Distinct Types of Cochlear Nonlinearity, Biophysical Journal (2020), https://doi.org/10.1016/j.bpj.2020.10.005

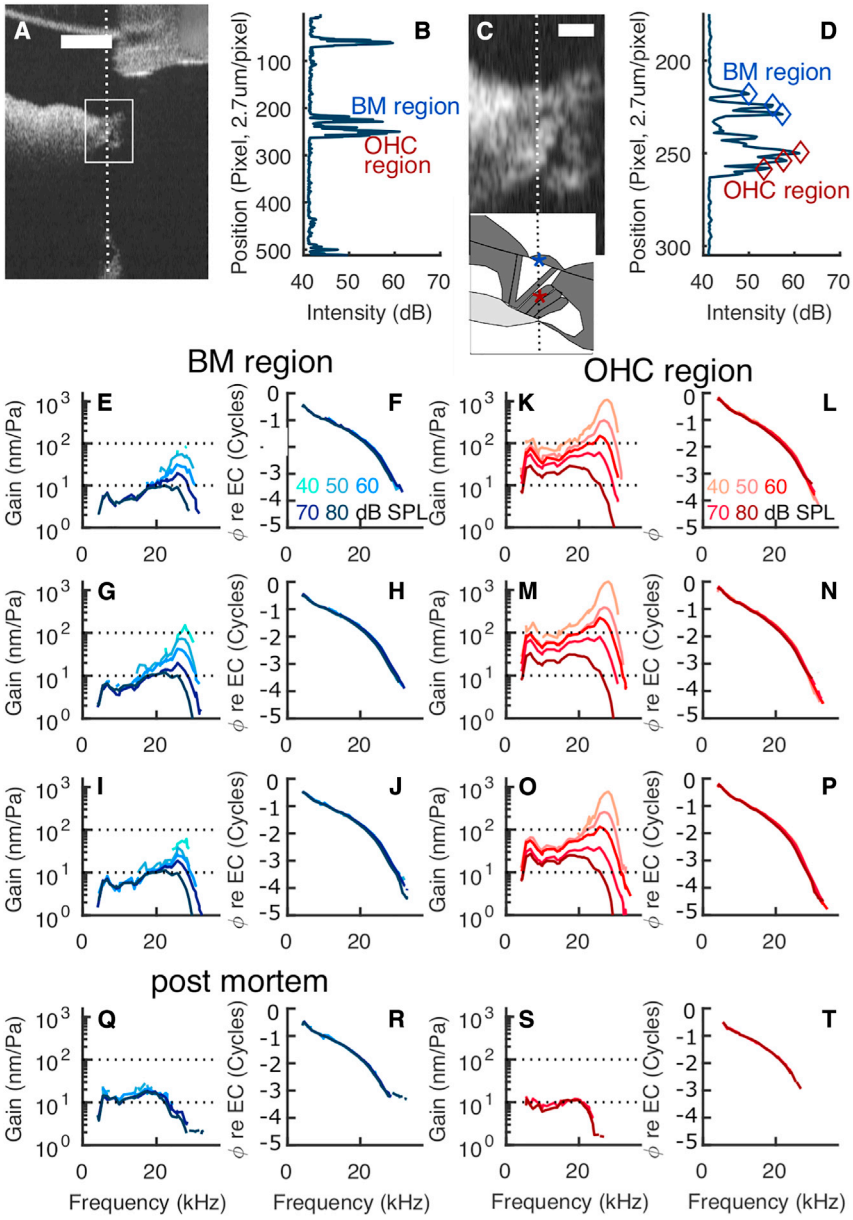

FIGURE 3 Measurement of cochlear vibrations with phase sensitive OCT. (*A*) B-scan image is shown. Scale bar, 250 μm. (*B*) Shown is an A-scan corresponding to the vertical line in (*A*); this is the line along which vibration measurements were made. The A-scan shows peaks at the round window membrane (*top* of A-scan) and in the BM and OHC regions. (*C*) Expanded view of B-scan is shown. Scale bar, 50 μm. Sketch underneath is an upside down and simplified version of Fig. 1 *B* and identifies BM and OHC regions with asterisks. In the B-scan, OHC and BM regions are identified using the dark fluid gaps and known anatomy. The classic cross-sectional anatomy is discernible but odd looking because the angle of approach was tilted from the classic histological view (29). (*D*) Shown is the expanded view of A-scan with locations in which vibration was analyzed identified with diamonds. (*E–J*) Shown is the gain and phase for EC pressure from the three diamond-identified points in the BM region of (*D*). (*K–P*) Shown is the gain and phase for EC pressure from the three diamond-identified points in the OHC region. The top BM region diamond corresponds to the data in the top gain and phase panels (*E* and *F*); the top OHC region diamond corresponds to the data in the top gain and phase panels (*K* and *L*), and so on. Darker shades indicate higher SPL, key in (*F* and *L*). (*Q–T*) Shown are responses in the two regions 10–15 min post mortem. Only the 70 and 80 dB stimuli gave displacements that were significantly above the noise threshold. Expt. 789, October 2, 2019. To see this figure in color, go online.

analysis on these short recordings in approximately 5 min and used the resulting coarse tuning curves to gauge the quality of the displacements at the selected location and to estimate the BF.

Experimental paradigm

After the positioning described above, we took a series of baseline measurements, each consisting of a set of DPOAE audiograms and vibration tuning curves. After these were completed, the gerbil was given an iv injection of furosemide (100 mg/kg) in the left femoral vein. A set of DPOAE measurements was taken immediately after the injection. When the injection was successful, the $2f_1 - f_2$ DPOAEs at 50 dB typically fell to the noise level, and the DPOAEs at 70 dB were greatly reduced in amplitude. A set of accompanying zwuis tuning curves was then taken. The measurements were repeated approximately every 10 min for up to 4 h postinjection. The DPOAE measurements took approximately 3 min each, and a complete set of tuning curves took approximately 4 min, primarily because of the time required, ~40 s, to transfer large raw files to a solid state drive. Because of the long time required for each experiment, some drift in the preparation was inevitable. Between recordings, we monitored the position of the cochlea with ThorImage and made minor adjustments to the position as needed. At the conclusion of the experiment, the animals were overdosed with pentobarbital. In some preparations, a set of post mortem tuning curves was acquired after the animal expired.

Electrophysiological recordings

The EP and microphonic potentials (termed LCM) were measured as described previously (16), and the results shown here are redrawn from that study as they provide important background and comparative information. The LCM was measured with an insulated tungsten electrode (tip diameter of ~1 μm; FHC, Bowdoin, ME) inserted into scala tympani and

Please cite this article in press as: Strimbu et al., Manipulation of the Endocochlear Potential Reveals Two Distinct Types of Cochlear Nonlinearity, Biophysical Journal (2020), https://doi.org/10.1016/j.bpj.2020.10.005

advanced close to the BM at the base of the cochlea, close to the 18 kHz location. The LCM was measured in response to pure-tone stimuli. The voltages were amplified 500–1000× (EG&G PARC) and recorded with the TDT system. The EP was measured with an ∼10 μm diameter glass microelectrode with an Ag/AgCl pellet and filled with 0.5 M KCl. The reference electrode was filled with standard saline and was placed on the muscle of the right leg. The DC signal was amplified 10× and recorded every second with a usb DAQ board (DATAQ Instruments, Akron, OH).

RESULTS

A total of 13 gerbils, 9 male and 4 female, were used in this study. All exhibited healthy baseline DPOAEs and OCC vibrations. Five preparations showed significant, and in three cases nearly complete, recovery of vibration responses. Results from the two that showed the most complete recovery are shown in detail, and results from two others are shown in grouped data. In the other well-recovered preparation, recovery could not be tracked because of mechanical drift in the apparatus. Four animals showed only partial recovery and died between 50 and 100 min after the injection. Finally, in three experiments, the iv injection was not successful, and in one, no recovery occurred in the BF region.

The primary measurement of this study was that of vibration within the OCC during recovery from furosemide-induced reduction of EP. Sound stimuli consisted of multitone "zwuis" stimuli, in which at each amplitude level, all tones are delivered simultaneously. The tuning observed with multitone stimuli is similar to that with pure-tone stimuli, but nonlinearity is more pronounced, likely because of the increased sound volume (21,30). We concentrated on two regions within the OCC, the BM and the OHC regions, as shown in introductory Fig. 3. The two regions can be found based on the surrounding fluid-filled regions of the inner and outer tunnels of Corti, which are dark in the B-scan (see Fig. 1 *B* for anatomical labels). The outer tunnel is distinct, and the inner tunnel between the pillars is less distinct in the Fig. 3 B-scan but still detectable. The vertical line in the B-scan indicates the location of the A-scan in which motion was measured, and the SD-OCT technique makes simultaneous motion measurements at all locations in the A-scan. In Fig. 3, *E–J*, motion responses are shown from three points within the BM region; in Fig. 3, *K–P*, responses are shown from three points within the OHC region. The spacing between the BM region and OHC region was typically ∼60 μm. Both BM and OHC region displacements were tuned and nonlinear, but the OHC region responses were up to an order of magnitude larger than BM responses; compressive nonlinearity in the BM responses began ∼1/2 octave below the BF, whereas in the OHC region nonlinearity extended throughout the entire frequency range. These findings are similar to previous measurements obtained by OCT and interferometry (21,29,31–33). The intraregion differences in vibration were small compared to interregion differences. This is an important point because motion results are most reliable when taken from a local maxima in the A-scan (34); in the hours-long furosemide study, the preparation and image underwent small shifts, and therefore, the exact same points were not probed during the course of the experiment. The phases in both regions show the familiar traveling wave delay through several cycles. The OHC region phases led the BM region phases by ∼0.02 cycles at 5 kHz, reducing to ∼0.01 cycles at 10 kHz and could lag slightly at frequencies above 20 kHz. Phase differences and time variations with furosemide will be shown and discussed below; here, we simply show the basic shape. Responses measured 10–15 min post mortem are shown in Fig. 3, *Q–T*; both OHC and BM regions became linear and were either tuned broadly (BM) or nearly low pass (OHC region).

We used furosemide to reversibly reduce the EP as in Fig. 2 *A*. DPOAE was measured directly after the iv injection to confirm successful injection, and OCC vibrations recordings were taken immediately thereafter and repeated every 10 min. Data from the two preparations with the fullest recovery are presented in Fig. 4, which shows BM and OHC region tuning curves measured at select time points. Before the injection, baseline BM tuning curves were typical of healthy ears (*blue curves* in Fig. 4, *A* and *G*). The gains showed the characteristic peak at the BF (∼26 kHz for both of these preparations), a compressive nonlinearity at nearby frequencies, and linear growth for sub-BF frequencies, starting ∼1/2 octave below BF. As in Fig. 3, OHC region vibrations (red curves) exhibited higher amplitudes, or equivalently higher gains, than the BM vibrations and were compressively nonlinear across the entire frequency range tested. After the furosemide injection, the BM responses resembled those of a passive cochlea, with a broad peak and nearly linear tuning (*blue curves* in Fig. 4, *B* and *H*). The responses at 40 and 50 dB SPL often fell below the noise level. The BM responses in the linear region below the BF were essentially unaffected by the injection. These observations are similar to previous studies of the effects of furosemide on BM vibrations (12). After iv furosemide, the OHC region vibrations showed a decrease in amplitude, and the tuning became low pass. At the 26 kHz BF, responses at all SPLs were greatly reduced and had dropped to within the noise through 60 or 70 dB SPL. However, over the wide range of frequency in which responses were detectable, they retained compressive nonlinearity. Amplitude recovery proceeded over several hours. 50 min postinjection, the BF region BM and OHC vibrations remained depressed (Fig. 4, *D* and *J*), whereas sub-BF OHC vibrations had fully recovered in experiment (expt.) 785 (Fig. 4 *D*) and substantially recovered in expt. 788 (Fig. 4 *J*). 70 min after the furosemide treatment, the BF peak began to recover (Fig. 4, *E* and *K*). In expt. 785, both the BM and OHC vibrations had almost fully recovered at 120 min (Fig. 4 *F*), and in expt. 788, recovery was substantial at 120 min (Fig. 4 *L*). In this experiment, responses were

Please cite this article in press as: Strimbu et al., Manipulation of the Endocochlear Potential Reveals Two Distinct Types of Cochlear Nonlinearity, Biophysical Journal (2020), https://doi.org/10.1016/j.bpj.2020.10.005

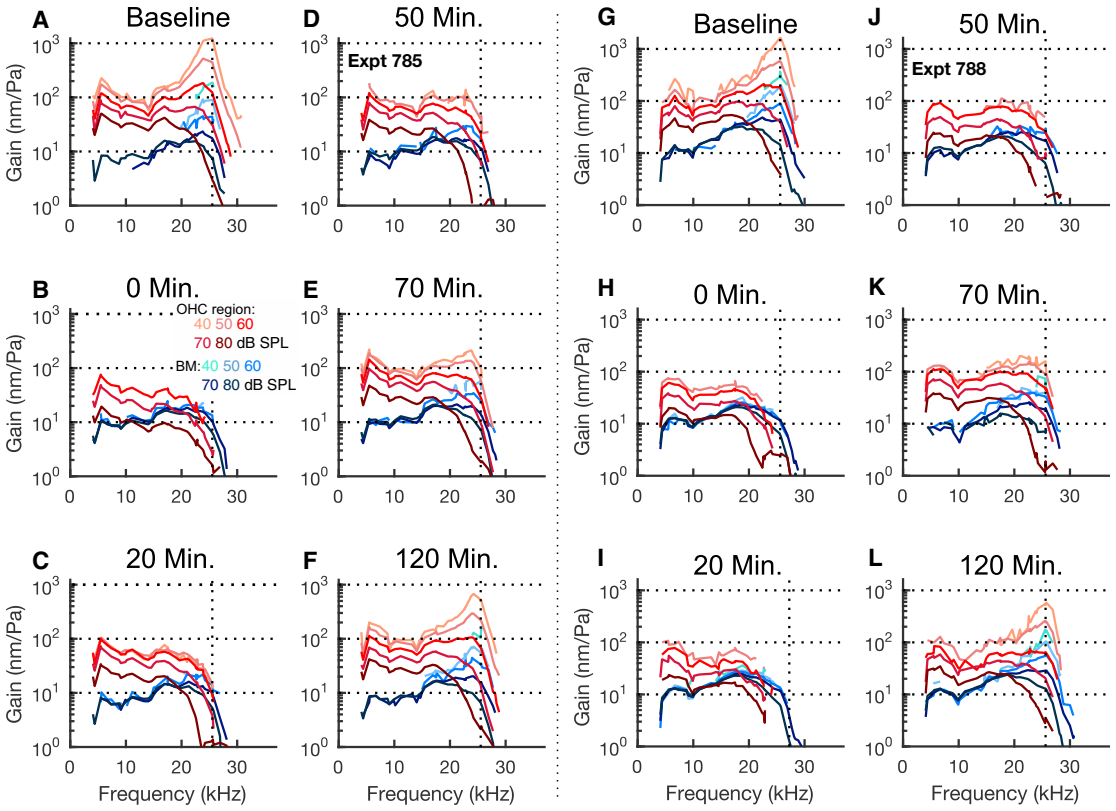

FIGURE 4 Loss and recovery of the BF displacement peak after furosemide injection. Vibration amplitude, normalized to the stimulus level in the ear canal (gain), is shown from the two preparations with the fullest recovery. BM/OHC region vibrations are plotted in blue/red with darker shades indicating higher SPL, key is in (*B*). (*A–E*) Expt. 785, August 28, 2019. (*G–L*) Expt. 788, September 17, 2019. (*A* and *G*) Baseline before furosemide is shown. (*B* and *H*) Immediately after iv furosemide is shown. (*C–F*) and (*I–L*) Shown is displacement gain at several time points after furosemide, with (*F*) and (*L*) the 120 min measurements, when recovery had plateaued. To see this figure in color, go online.

monitored for 250 min post-furosemide, but beyond the 120 min time point, the responses did not improve.

Fig. 5 shows the time variation of the vibration responses at BF and BF/2 for the two illustrative experiments. At BF/2, BM responses were unaffected by the furosemide treatment (Fig. 5, *C* and *G*). The OHC region BF/2 responses dropped by factors of 2–3 but retained nonlinearity even immediately post-furosemide. The OHC region BF/2 responses recovered nearly fully by 50 min for expt. 785 (Fig. 5 *D*); for expt. 788, the main recovery was by ~70 min and was not full at high SPL (Fig. 5 *H*). At BF, after furosemide, the BM responses dropped most at low SPL, and for both experiments at 40 and 50 dB SPL, they dropped beneath the noise floor (Fig. 5, *A* and *E*). There was considerable recovery at ~60–70 min, when these low SPL responses re-emerged and continued recovery to 100 min. The OHC region BF responses showed an even greater drop into the noise (Fig. 5, *B* and *F*), and by considering Fig. 4, this can be seen to be due to the low-pass character of the post-furosemide OHC region responses. In the OHC region, as in the BM region, recovery of amplification at the BF was well underway at ~60–70 min and continuing to 100–120 min. The time course of amplification recovery as measured in these BF vibration responses is similar to what was observed in LCM BF responses (16). To illustrate that similarity, LCM BF data are plotted along with OHC region curves in Fig. 5, *B* and *F*. The LCM data were scaled to overlie the vibration data, which does not affect the comparison since the *y* axis is logarithmic.

The DPOAE results for the two illustrative experiments are in Fig. 6. Before the furosemide injection the $2f_1 - f_2$ levels were typically 30–40 dB lower than the primaries and present up to $2f_1 - f_2 = 32$ kHz, the maximal frequency tested, when elicited with the 70 dB SPL primaries (Fig. 6, *B* and *D*.) With 50 dB SPL primaries, they were measurably present to $2f_1 - f_2 \sim 25$ kHz (Fig. 6, *A* and *C*). Just after furosemide, DPOAEs dropped into the noise level (~0 dB SPL) at all frequencies for the 50 dB primaries and at frequencies above $2f_1 - f_2 \sim 15$ kHz for the 70 dB primaries. After an early burst of recovery at relatively low frequencies (below 10 kHz), DPOAEs gradually increased and showed their fullest recovery at ~120 min, similar to the vibration. At that point, DPOAEs had recovered fully at $2f_1 - f_2$ frequencies below ~22 kHz, which corresponds to f_2 of ~32 kHz. The recovery of DPOAEs was nonmonotonic, and a boost of recovery at ~70 min is apparent, particularly in

Please cite this article in press as: Strimbu et al., Manipulation of the Endocochlear Potential Reveals Two Distinct Types of Cochlear Nonlinearity, Biophysical Journal (2020), https://doi.org/10.1016/j.bpj.2020.10.005

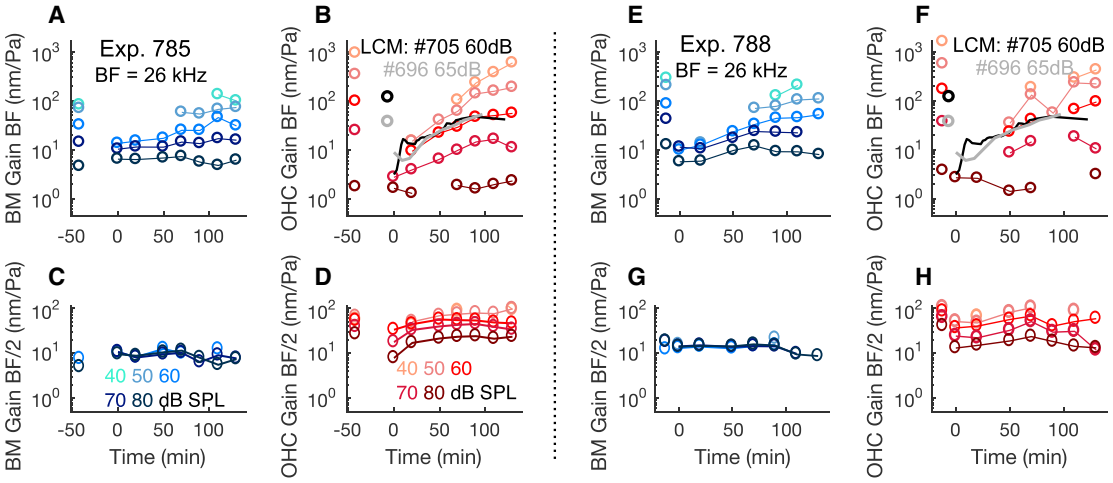

FIGURE 5 BM and OHC region vibration before, after, and during recovery from furosemide treatment, with time $t = 0$ right after the injection. Vibration amplitude, normalized to ear canal pressure (gain), is shown for the two preparations with the fullest recovery. (*A–D*) Expt. 785 and (*E–H*) Expt. 788 are shown. (*A* and *E*) BM gains at the BF. (*B* and *F*) OHC region gains at BF. (*C* and *G*) BM gains at BF/2. (*D* and *H*) OHC region gains at BF/2. Gaps in the data occur when the responses were within the noise. The relatively long time between baseline and $t = 0$ in expt. 785 is present because, as noted in methods, to present the fullest (least noisy) baseline measurement data set, the set used for illustration was not always just before the injection. The gray-scale data in (*B*) and (*F*) are BF LCM results from the precursor study (16). These data illustrate that BF LCM and OHC region vibration responses recovered on a similar timescale. The *y* axis for the LCM data have units mV/Pa and have been scaled by factors of 60 (expt. 705) and 40 (expt. 696). To see this figure in color, go online.

the range of f_2 from 20 to 30 kHz, which encompasses the 26 kHz BF of the vibration measurements. DPOAEs are thought to come primarily from the frequency regions of f_2, and $2f_1 - f_2$, and the OP shifts (recall Figs. 1 *C* and 2 *B*) that affect nonlinearities like DPOAEs have been observed to vary with cochlear location (23). To observe the time dependence of the DPOAE in the BF frequency region more clearly, in Fig. 6 *E* the recovery time course of an average of three DPOAEs from three adjacent frequencies around $f_2 = 30$ kHz are shown as line plots. Fig. 6 *E* is from experiments 785 and 788; Fig. 6 *F* is a mean of the four preparations in which the vibration's BF peak recovered most fully. The reduction at $t = 0$ corresponds to the dark line that appears at $t = 0$ in the heat plots of Fig. 6, *A–D*. After that sharp reduction, the DPOAEs underwent 20 min of rapid recovery but then dropped again, reached a local minimum at 50 min, and then entered a final recovery phase. Fig. 6 *G* shows DPOAE results from the precursor study (16). In that study, DPOAE was measured not immediately after furosemide but ~4 min later, and the initial sharp drop is less pronounced, but the rapid recovery followed by a decline and final recover after 50 min is similar. The size of the DPOAEs is expected to be directly affected by the reduction in EP, which would reduce OHC receptor current and voltage and thus reduce active cochlear feedback. However, the nonmonotonic recovery illustrated in Fig. 6, *E–G* cannot be attributed to the EP, which recovers monotonically and had stabilized at ~40 min post-furosemide (Fig. 2 *A*; (16)).

In four preparations, recovery after furosemide never became substantial. An example is in Fig. 7. The reduction just post-furosemide was similar to what was observed in Fig. 4. The sub-BF wideband nonlinearity in the OHC region was retained just after furosemide, but the BF peak was absent. At 20 min, the BF peak just began to emerge in the OHC and BM regions, but the recovery faltered at 50 min, when the BM responses were nearly linear, and the OHC region, while retaining wideband nonlinearity, has returned to a low-pass state. Responses continued to decline and, at 90 min, had declined greatly, yet wideband nonlinearity in the OHC region remained. Fig. 7, *G* and *H* show the DPOAEs evoked by the 70 dB SPL primaries from this experiment. As shown by the heat map in Fig. 7 *G*, after the furosemide injection, the DPOAEs showed a sharp reduction at all frequencies followed by a brief, substantial recovery over ~20 min, but the high-frequency BF region exhibited a steady decline thereafter. Fig. 7 *H* shows the brief recovery and subsequent decline in the mean of three DPOAEs around $f_2 = 30$ kHz.

Fig. 8 takes a further look into the sub-BF behavior in the four preparations with good recovery and the four preparations in which recovery faltered. Responses at BF/2 are shown, and the initial time period is emphasized, during which EP would have dropped and potentially recovered to a stable level. Fig. 8, *A* and *B* are from the four better-recovered preparations; Fig. 8, *C* and *D* are from the four poorly recovered preparations. The left panels show the 70 dB responses over time; this SPL was chosen to include many time points and to be a SPL, where at BF/2, responses always were above BM responses so remained influenced by cochlear activity. The right panels are grouped data at 60, 70, and 80 dB SPL. Referring to the EP data of Fig. 2 *A*, we expect

Please cite this article in press as: Strimbu et al., Manipulation of the Endocochlear Potential Reveals Two Distinct Types of Cochlear Nonlinearity, Biophysical Journal (2020), https://doi.org/10.1016/j.bpj.2020.10.005

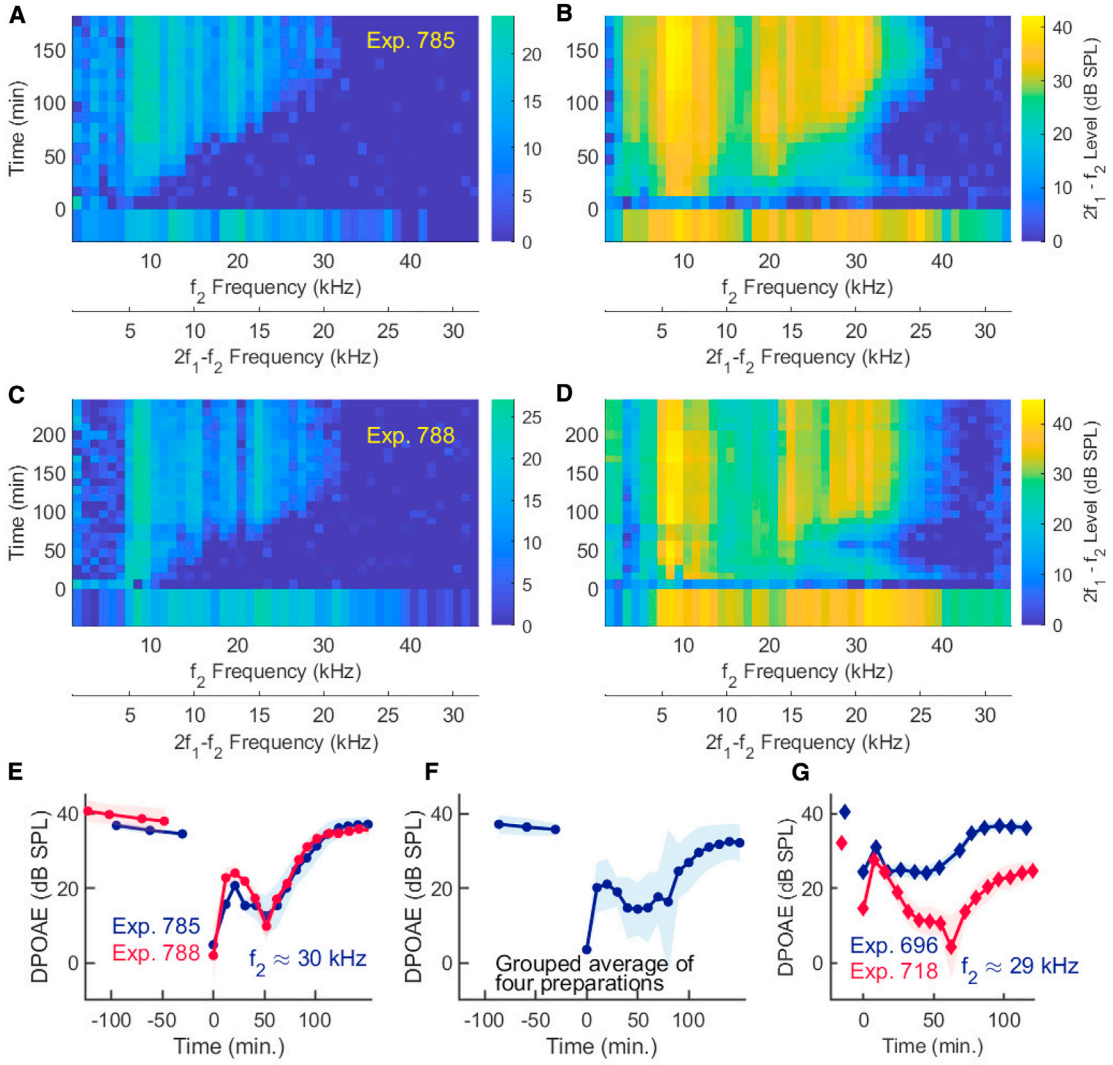

FIGURE 6 Recovery of DPOAE. (*A–D*) show the full frequency range of $2f_1 - f_2$ DPOAE levels for Expt. 785 (*A* and *B*) and Expt. 788 (*C* and *D*). DPOAEs were evoked by 50 dB SPL (*A* and *C*) and 70 dB SPL (*B* and *D*) primaries, with $f_2/f_1 = 1.2$. The two *x* axes indicate both the $2f_1 - f_2$ and the f_2 frequencies. Note the sharp drop immediately after the injection at $t = 0$ min and the gradual recovery that reached its maximum at ~120 min. (*E*) Three DPOAEs around $f_2 = 30$ kHz, corresponding to DPOAE frequencies ~21 kHz, were averaged, and the mean and SD are shown. Primary levels were 70 dB SPL. (*F*) Shown are results as in (*E*), averaged over the four preparations with substantial recovery (Expts. 780, 783, 785, and 788). (*G*) DPOAE recovery from the precursor study (16) shows that the time course of recovery was similar in the two studies. In (16), after furosemide, LCM was measured before DPOAE; thus, the $t = 0$ point is missing. Other minor differences are as follows: $f_2/f_1 = 1.25$, primary levels were 65 dB SPL, and f_2 extended to only 30 kHz. To see this figure in color, go online.

that EP is ~−20 to −10 mV at the $t = 0$ point of the displacement measurement, down from a healthy +80 mV value. The resting potential of an OHC is ~−60 mV, so the driving voltage for OHC current will have been reduced from its healthy ~140 mV value to ~40–50 mV, a reduction of a factor of approximately three. If the observed sub-BF motion were purely due to OHC electromotility with the OHC current drive reduced by a factor of three post-furosemide, one would expect a reduction in vibration of a factor of three. The reductions in Fig. 8 from pre-furosemide to the $t = 0$ value are on average about a factor of two. The factor of three expectation is approximate because sound-induced motion will provide a bound on the reduction of motion, and changes in MET OP muddy the simple expectation. However, it is clear that when EP dropped substantially, the sub-BF OHC region motion dropped substantially, and as EP recovered (from Fig. 2 over ~40 min), the sub-BF motion recovered. In the preparations that showed poor recovery (Fig. 8, *C* and *D*), the recovery in sub-BF responses faltered at 50 min, like the faltered recovery observed in the BF peak (Fig. 7). This sputtering recovery could be due to a reversal in the recovery of EP or the reversal of some other formerly recovering property because of a general decline in the condition of the preparations.

Returning to the preparations with good recovery, we consider the changes and recovery in the phase responses. Data are shown from the two experiments in Fig. 4 and a

Please cite this article in press as: Strimbu et al., Manipulation of the Endocochlear Potential Reveals Two Distinct Types of Cochlear Nonlinearity, Biophysical Journal (2020), https://doi.org/10.1016/j.bpj.2020.10.005

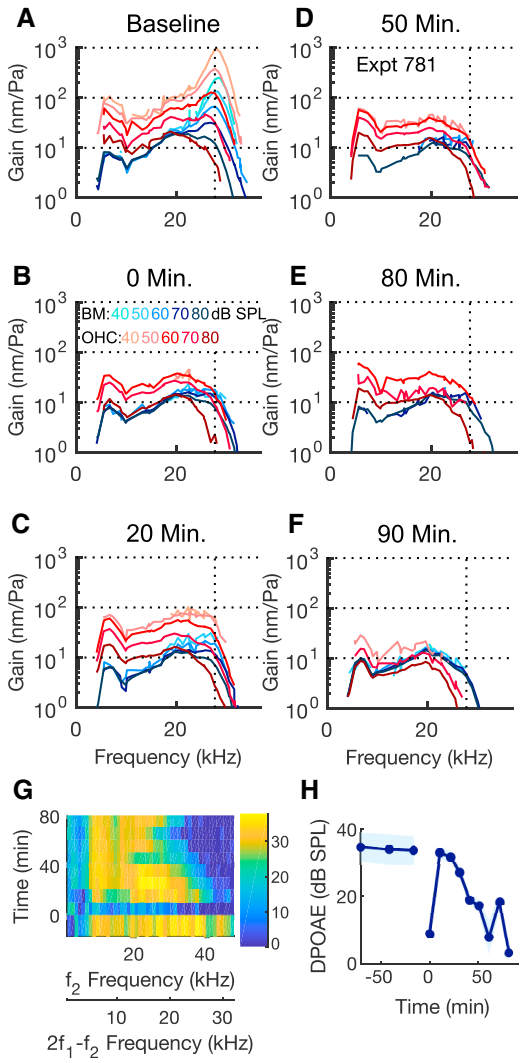

FIGURE 7 BM and OHC vibration after furosemide in one of the preparations that did not recover substantially (Expt. 781). Vibration amplitude is plotted referenced to ear canal pressure (gain). (*A*) Baseline before furosemide is shown. (*B*) Immediately after iv furosemide is shown. (*C–F*) Shown is the displacement gain at several time points, with (*F*) the final, 90-min measurement. (*G*) Full range of $2f_1 - f_2$ DPOAE levels is evoked with 70 dB SPL primaries. Color bar to the right is level in dB SPL. (*H*) Three DPOAEs around $f_2 = 30$ kHz, corresponding to DPOAE frequencies ~21 kHz, were averaged, and the mean and SD are shown. Primary levels were 70 dB SPL. To see this figure in color, go online.

third experiment (783). The top row of Fig. 9, *A*, *C*, and *E* shows baseline phase data and illustrates that BM and OHC region phases go through a similar traveling wave excursion of several cycles. The second row (Fig. 9, *B*, *D*, and *F*) explores OHC-BM phase differences and how they change in time. In the baseline condition at low frequency (a few kHz), OHC region vibration phase led BM phase by up to ~0.2 cycle. The phase lead declined with frequency to eventually become a lag of ~0.1 cycle close to the BF. Just after furosemide, the OHC-BM phase difference dropped by ~0.05 cycle (18°) across frequency in the data of Fig. 9 *B* and that observation approximately holds for the other two preparations in Fig. 9, *D* and *F*. During the recovery period, that general-frequency drop in OHC-BM phase difference was partially but never fully reversed. In Fig. 9 *G*, phase differences within each region before and just after furosemide are shown. This is grouped data with mean and SD from all eight preparations. The BM phase changed little, and thus, most of the time-dependent phase differences seen in Fig. 9, *B*, *D*, and *F* resulted from changes in the OHC region phase.

DISCUSSION

The electrical gradient of the EP provides much of the driving force for the MET currents. In the OHCs, the receptor potentials generated by these currents drive electromotility, which boosts OCC vibrations and is an essential component of the cochlea's active process. We used furosemide to reduce EP and followed the recovery of OCC vibrations and DPOAEs over several hours. BM and OHC region vibrations recovered nearly fully in several preparations, and the timescale of recovery in different frequency regions and in DPOAEs indicates that several processes are involved in recovery. OHC region sub-BF vibration retained wideband nonlinearity throughout and was back to baseline by ~60 min, signifying relatively rapid recovery of robust electromotility. The recovery of the BF peak in the OHC region and at the BM, signifying functional cochlear amplification, occurred later, mainly during the time period between 70 and 120 min. This two-stage recovery is reminiscent of the findings of Wang et al., who studied changes in LCM following the same iv furosemide protocol (16). In that study, EP had stabilized at a subnormal level at ~40 min, and the LCM BF peak finally recovered at 100 min or later. The timing of changes in LCM harmonic responses indicated that the recovery of cochlear amplification occurred simultaneously with recentering of the MET channel OP. In this study of OCC vibration, DPOAEs were used to explore OP shifts. In Fig. 6, *E* and *F*, the $2f_1 - f_2$ DPOAE from the same frequency region as the BF of the vibration measurements initially dropped steeply, had a local maximum at ~20 min, dropped to a local minimum at ~50 min, and then began a final recovery, stabilizing at the pre-furosemide level by 120 min. Fig. 6 *G* shows that the DPOAE recovery in (16) followed a similar pattern. These results can be considered through the lens of the MET OP behavior found in (16). In Fig. 10 *A*, the MET function that was derived in (16) is shown with zero OP offset, and with offsets of −0.12 and +0.05 Pa. These offsets are included because in the previous findings included in Fig. 2 *B*, the MET OP was positive at a value of ~0.05 Pa at $t = 0$, shifted negative to a minimal value of ~−0.12 Pa at ~60 min, and began to recenter (shift toward zero) at ~60–70 min. Fig. 10 *B* shows how the size of the $2f_1 - f_2$ distortion produced by the nonlinearity in Fig. 10 *A* is

Please cite this article in press as: Strimbu et al., Manipulation of the Endocochlear Potential Reveals Two Distinct Types of Cochlear Nonlinearity, Biophysical Journal (2020), https://doi.org/10.1016/j.bpj.2020.10.005

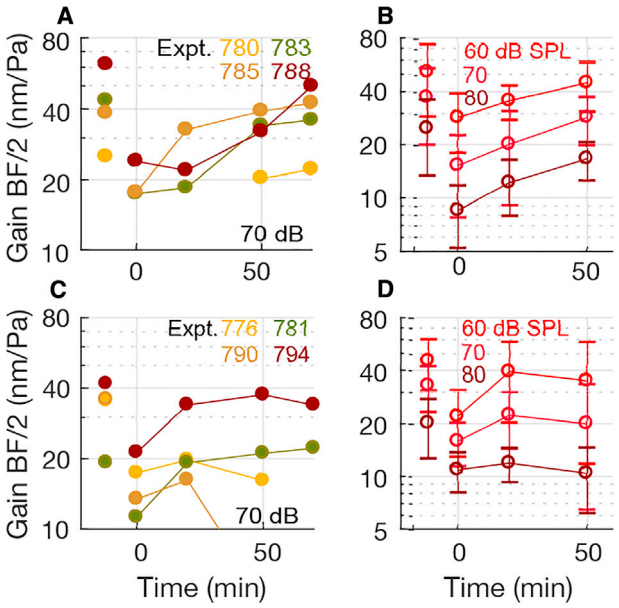

FIGURE 8 Reduction and early recovery of OHC region sub-BF (BF/2) vibration after furosemide. Vibration is shown referenced to ear canal pressure. (*A* and *B*) Shown are results from the four preparations with the fullest recovery; (*C* and *D*) four preparations with poor recovery are shown. (*A* and *C*) 70 dB SPL results from the individual preparations are shown. (*B* and *D*) show the mean and SD of each set of four at 60, 70, and 80 dB SPL. The initial post-furosemide drop in vibration is around a factor of two for all eight preparations. Recovery faltered in the preparations with poor recovery. To see this figure in color, go online.

affected by OP shifts (7,23). The primary inputs into the nonlinearity were at a level of 70 dB SPL (0.06 Pa peak) to coincide with the primary inputs producing the DPOAEs in Fig. 6. Fig. 10 *B* shows that the $2f_1 - f_2$ distortion product is a maximum with 0 offset, is near zero at an offset of $\sim \pm 0.012$ Pa, and then increases as the absolute value of the offset increases. Thus, the second minimum in the DPOAE responses starting its descent at ~25 min in Fig. 6 and second boost of DPOAE recovery starting at ~50 min is likely due in large part to MET OP shift. It is worth underlining that between 50 and 100 min is also when the BF peak underwent its steady recovery in BM and OHC region responses, tying the recovery of cochlear tuning to the OP shift.

For completeness, we discuss the phase time variations, although they end up not being very illuminating. In past work, simultaneous pressure and voltage measurements indicated that a phase shift between LCM and BM displacement was critical for OHC forces to be phased to provide power input to the traveling wave (20), and we explored this data for time dependence in the vibration phase after furosemide and recovery (Fig. 9, *B*, *D*, and *F*). As a broad-brush observation from these experiments, after furosemide, the OHC-BM phase difference was offset by ~ -0.05 cycle ($-18°$). This offset reduced the sub-BF phase lead of OHC region relative to BM and increased the BF region phase lag of OHC region relative to BM. During the recovery of amplification, the most compelling phase recovery came from expt. 788 (Fig. 9 *B*) in which, in the 70–120 min during which amplification recovered, this 18° furosemide-induced offset fully reversed at frequencies above 13 kHz. Thus, in this experiment, the phasing between OHC and BM motion returned to a pre-furosemide character, concurrent with recovery of amplification. Expt. 785 also underwent a furosemide-induced negative offset in OHC-BM phase, and the offset recovered but only partially, although amplification showed substantial recovery. Expt. 783 also underwent a furosemide-induced negative offset in OHC-BM phase, and in this case, the offset recovered barely at all. In expt. 783, amplification recovery, although substantial, was less full than in the other two preparations. In sum, an OHC-BM phase change was robust after furosemide—a downward offset occurred between the baseline and $t = 0$ measurements in three of three explored data sets. Recovery of that offset was only weakly correlated with recovery of amplification. In the study of Cooper et al. (29), the phase of OHC vibration relative to BM was found to be viewing-angle dependent, and subtle preparation-viewing angle differences could conceivably be affecting the repeatablity of phase changes in our study.

We end by discussing how this set of findings ties in with previous literature and speaks to the key questions. What is required for functional cochlear amplification and for the production of the compressively nonlinear BF peak? What is essential, and what is sufficient? We showed in (16) that a normal EP is not essential for recovery of the BF peak, and recovery of cochlear amplification at subnormal EP had been hypothesized previously based on DPOAE recovery (17). We showed in (16) that recovery of the BF peak after furosemide occurred along with an OP shift, and that finding is reinforced by the DPOAE findings of this report. These findings lend strength to the expectation that beyond the size of critical factors such as driving voltage and electromotility, the healthy BF peak relies on qualitative conformational factors. That concept was illuminated by Jacob et al. (35), who applied quasistatic current injections to restore the EP in situ in guinea pig temporal bone preparations. Using confocal fluorescent microscopy and interferometry, they found that the organ of Corti underwent a series of mechanical conformational changes, shifting the apical region of the OHCs toward scala vestibuli, and these shifts positioned the system into a region of increased sensitivity. The position changes, ~50–100 nm, are smaller than the resolution of an OCT when used in two-dimensional (B-scan) imaging mode, so we cannot probe those findings directly with our imaging system. The recovery of the BF peak we observed occurred after EP was likely substantially recovered and stabilized, whereas the changes observed by Jacob et al. (35) were concurrent with directly induced EP changes. Despite this difference, the two studies are similar in the observation that adjustable conformation seems to set

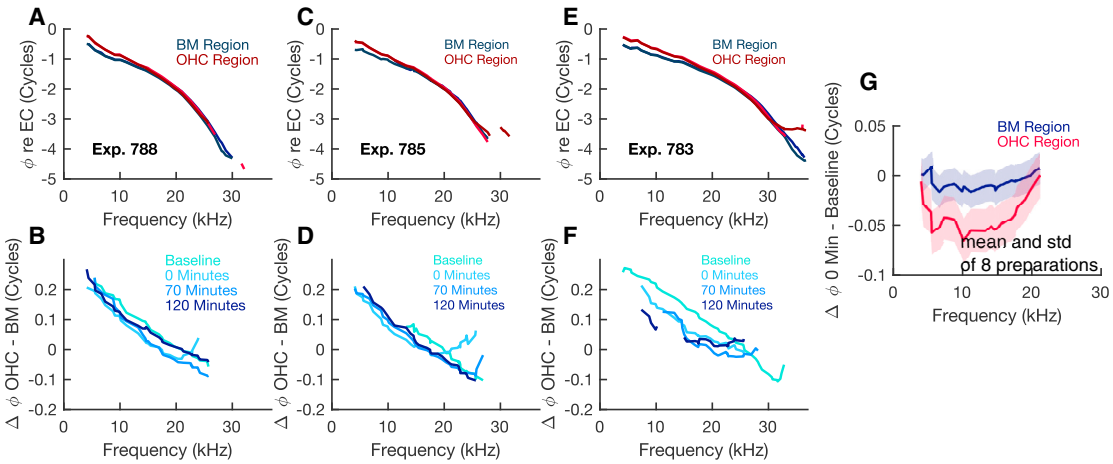

FIGURE 9 Phase differences and changes with recovery from furosemide. Only relatively high SPL results are shown (70 and/or 80 dB SPL) because at lower SPL, data could drop beneath the noise floor after furosemide. (*A*, *C*, and *E*) Shown are baseline phase data from Expts. 785 and 788 (Fig. 4) and a third (Expt.783) that showed substantial recovery. This row reinforces the basic similarity and small but robust differences between BM and OHC region phases at baseline. Shown are 70 and 80 dB SPL results, with color coding as in Fig. 4. (*B*, *D*, and *F*) Shown are phase differences between OHC region and BM region, before and just after furosemide, at 120 min, when recovery was approximately fullest and at one intermediate time point (70 min). 70 dB SPL results are shown. A three-point smoothing was done on these data to reduce distracting sharp variations. (*G*) Shown are phase differences within each region before and just after furosemide. Mean and SD shown from the eight preparations of Fig. 8. 80 dB SPL results are shown. BM region phase changed little, and most of the time-dependent phase differences resulted from changes in OHC region phase. To see this figure in color, go online.

the proper mechanical conditions for healthy cochlear function. This observation is related to the concepts of automatic gain control and parametric impedance regulation, in which real-time transformations are used as a mechanism for producing the BF peak (29,36). In this article, the conformational changes giving rise to OP shifts occurred over minutes in concert with recovery of the BF peak and do not obviously support the real-time transformations involved in automatic gain control, but they do underscore the importance of conformation for cochlear tuning.

The main new finding of this report was that robust, wideband nonlinearity—evincing robust wideband OHC electromotility—is present throughout the recovery period after iv furosemide and can fully recover an hour before the recovery of the BF peak. Thus, although OHC electromotility is essential for producing the BF peak (37), the current observations show that robust electromotility is not in itself sufficient for producing the BF peak, and the observed conformational recovery is not simply producing the recovery of electromotility. This eliminates some possibilities for what is driving the final recovery of the BF peak. For example, noise damage leading to a temporary threshold shift causes the stereocilia to become transiently uncoupled from the TM (26), but if the response and recovery after iv furosemide were due to uncoupling and recoupling of the OHCs to the TM, one would expect OHC electromotility to recover in step with the BF peak, not the observed hour earlier. Reduced EP might decrease calcium entry into the stereocilia, raising the open probability of the MET channels and affecting the adaptation processes that influence stereocilia mechanics (38–41) and possibly cochlear amplification (3,5,42). Using organ of Corti explants, Vélez-Ortega et al. showed that reducing calcium entry into the bundles for as little as 1 h caused contraction of the shorter rows that contain the transduction channel and its associated machinery (27). If a similar effect occurs in vivo in an adult animal, changes could occur to the hair bundles during the 30–40 min after the furosemide injection when the EP remains significantly depressed, and such physical changes would likely recover over a longer timescale than the recovery of EP. However, these changes would reduce OHC MET current and thus electromotility—and the persistent wideband nonlinearity we observed indicates that electromotility was functioning through the recovery period. Thus, the delayed recovery of the BF peak is likely not due to a recovery of gross hair bundle morphology but might be due to more subtle recovery affecting the MET channel and stereocilia mechanics.

After reduced EP because of iv furosemide or the similarly acting iv ethacrynic acid, endolymphatic concentrations of K^+, Cl^-, Ca^{2+}, and Na^+ are altered and recover later than EP (43–46). For example, after 100 mg/kg iv furosemide in guinea pig, [Cl^-] dropped by ~20 mM over 20 min and, after a stable period, recovered over 40 min, during a time when EP was almost fully recovered (44). Perturbation to perilymphatic [Cl^-] affects cochlear amplification, presumably because of the significance of chloride in the electromotile function of prestin (47). However, it seems unlikely that recovery of prestin function is responsibly for the delayed BF peak recovery we observe because electromotility appears to have been robust during the entire recovery period. The physical properties of the gelatinous TM are sensitive to its ionic environment (48–50), and the TM might be key to the recovery process after furosemide.

Please cite this article in press as: Strimbu et al., Manipulation of the Endocochlear Potential Reveals Two Distinct Types of Cochlear Nonlinearity, Biophysical Journal (2020), https://doi.org/10.1016/j.bpj.2020.10.005

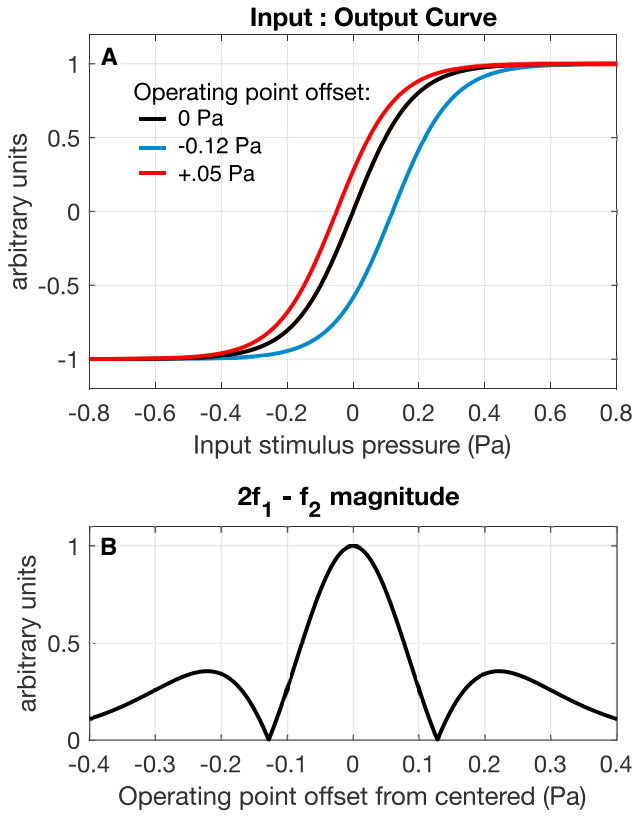

FIGURE 10 OP shifts in model MET input/output function and predicted the effect on DPOAE magnitude. (*A*) A two-state Boltzmann function representing the MET channel (Fig. 1 *C*) was fit in (16) using LCM measured just after furosemide, when feedback activity (amplification) was small or absent. $V = -V_{sat} + (2V_{sat}/(1 + \exp z(P + OP)))$. (*V*) is LCM, (*P*) is ear canal pressure, (*OP*) is operating point, and the slope factor $z = -11.18$ Pa^{-1}. The function has been plotted here on a normalized scale, with $V_{sat} = 1$. The OP shift that occurred after iv furosemide was shown in Fig. 2 *B*. The most extreme OP offsets, −0.12 Pa and +0.05 Pa, are plotted in (*A*). (*B*) Using the Boltzmann function, the size of the $2f_1 - f_2$ generated by this simple nonlinearity is found for a range of OPs. The input SPL of f_1 and f_2 was taken as 70 dB SPL (0.06 Pa) to allow comparison between model predictions and the DPOAE results of Fig. 6, *E* and *F*. To see this figure in color, go online.

In addition to its role in pivoting stereocilia, the TM has been invoked as a core component of cochlear amplification, with its gelatinous structure acting as a mass in a resonant system (51–53) or as a wave-supporting structure in dual traveling wave models (54,55). Either of these roles could be temporarily disrupted by changes in its physical properties. Studies in mouse models with modified TM reinforce the sensitivity of cochlear mechanics to the TM's physical properties (56). In vitro, substitution of Na^+ for K^+ ions leads to swelling of the TM (48). The reported in vivo changes of endolymphatic [Na^+] after ethacrynic acid (45) and [K^+] after furosemide (43) are on the order of 10 mM, which is much smaller than what was studied in vitro, but subtle changes in the shape of the TM could alter the equilibrium position of the MET channel complex or be significant in other ways. After 60 mg/kg iv furosemide in guinea pig, endolymphatic [Ca^{2+}] increased from 20 to 300 μM with no apparent recovery over the 30-min recording period, although EP had substantially recovered (46). In an in vitro study, a 100-fold increase in [Ca^{2+}], from 20 to 2000 μM, produced ~7% shrinkage in the TM (50), so the reported 15-fold increase in [Ca^{2+}] after furosemide (46) could cause significant changes in TM conformation and function. Continuing in the vein of Ca^{2+} and the TM, in an in situ study, Strimbu et al. found that the calcium concentration in the TM is elevated relative to the bulk endolymph. After a brief exposure to loud sounds, both the TM calcium and cochlear microphonic were reduced and recovered in synchrony on a timescale of ~30 min (57). To summarize this section, the timescale of endolymph ionic concentration changes after reduced EP, the sensitivity of the TM to these ions, and the well-known and theorized roles of the TM in cochlear mechanics add to forward a hypothesis that the TM's particular physical state is key to the production of the BF peak. Future work will explore this hypothesis.

Finally, in addition to reducing the EP, furosemide may reduce auditory sensitivity through other mechanisms. Loop diuretics weaken the blood labyrinth barrier by damaging the tight junctions lining the stria vascularis, an effect that has been exploited to enhance the uptake of contrast agents in magnetic resonance imaging studies (58). The ototoxicity of other agents such as cisplatin or aminoglycosides increases when administered simultaneously with loop diuretics such as furosemide, likely because of the increased permeability of the drugs in the perilymphatic spaces of the cochlea (59). Furosemide applied extracellularly to isolated OHCs diminishes nonlinear capacitance, a surrogate for electromotility (60). More generally, furosemide is known to affect the biophysical properties of lipids in vitro (61). Such changes to the lipid bilayer of the hair cells' bodies could alter electromotility or the properties of the MET channels themselves (62,63). However, the concentrations of furosemide in perilymph (64) and endolymph (65) after iv injections at the dosages used in this study are in the micromolar range, approximately an order of magnitude lower than the extracellular concentration needed to evoke changes in nonlinear capacitance (60) or lipid properties in vitro (61). This suggests that any direct effects furosemide might have on the OHC bodies would be secondary in importance to the reduction of the EP.

In summary, we used the reversible changes caused by iv furosemide to probe the essential ingredients of cochlear amplification. After furosemide, the BF peak disappeared in BM and OHC region vibration responses, whereas the sub-BF OHC region retained wideband nonlinearity. Sub-BF OHC region responses substantially or fully recovered to baseline levels during the first hour after furosemide. This suggests that OHC electromotility was fully operational at that point, and based on recent findings from our

group, EP would have been stable at a subnormal level. The BF peak, signifying healthy cochlear amplification, underwent its own significant recovery during the second hour after furosemide, concurrent with an apparent recentering of MET channel OP. These findings indicate that the presence of normal, high EP is not necessary for amplification and robust OHC electromotility is not by itself sufficient for healthy cochlear amplification and support the idea that the adjustable mechanical conformation of the OCC is key to a functioning cochlear amplifier.

AUTHOR CONTRIBUTIONS

C.E.S. performed OCT experiments, analyzed the data, and drafted the manuscript. Y.W. performed iv injections in initial experiments and contributed to study design. E.S.O. supervised research, analyzed data, and participated in manuscript writing.

ACKNOWLEDGMENTS

This work was funded by National Institutes of Health grant R01-DC015362 and the Emil Capita Foundation.

REFERENCES

1. Ashmore, J. 2008. Cochlear outer hair cell motility. *Physiol. Rev.* 88:173–210.
2. Robles, L., and M. A. Ruggero. 2001. Mechanics of the mammalian cochlea. *Physiol. Rev.* 81:1305–1352.
3. Hudspeth, A. J. 2008. Making an effort to listen: mechanical amplification in the ear. *Neuron.* 59:530–545.
4. Ashmore, J., P. Avan, …, B. Canlon. 2010. The remarkable cochlear amplifier. *Hear. Res.* 266:1–17.
5. Peng, A. W., and A. J. Ricci. 2011. Somatic motility and hair bundle mechanics, are both necessary for cochlear amplification? *Hear. Res.* 273:109–122.
6. Fettiplace, R., and K. X. Kim. 2014. The physiology of mechanoelectrical transduction channels in hearing. *Physiol. Rev.* 94:951–986.
7. Brown, D. J., J. J. Hartsock, …, A. N. Salt. 2009. Estimating the operating point of the cochlear transducer using low-frequency biased distortion products. *J. Acoust. Soc. Am.* 125:2129–2145.
8. Lukashin, A., and I. Russell. 1997. A descriptive model of the receptor potential nonlinearities generated by the hair cell mechanoelectric transducer. *J. Acoust. Soc. Am.* 103:973–980.
9. Keithley, E. M. 2020. Pathology and mechanisms of cochlear aging. *J. Neurosci. Res.* 98:1674–1684.
10. Tu, N. C., and R. A. Friedman. 2018. Age-related hearing loss: unraveling the pieces. *Laryngoscope Investig. Otolaryngol.* 3:68–72.
11. Yamasoba, T., F. R. Lin, …, K. Kondo. 2013. Current concepts in age-related hearing loss: epidemiology and mechanistic pathways. *Hear. Res.* 303:30–38.
12. Ruggero, M. A., and N. C. Rich. 1991. Furosemide alters organ of corti mechanics: evidence for feedback of outer hair cells upon the basilar membrane. *J. Neurosci.* 11:1057–1067.
13. Sewell, W. F. 1984. The effects of furosemide on the endocochlear potential and auditory-nerve fiber tuning curves in cats. *Hear. Res.* 14:305–314.
14. Kusakari, J., I. Ise, …, R. Thalmann. 1978. Effect of ethacrynic acid, furosemide, and ouabain upon the endolymphatic potential and upon high energy phosphates of the stria vascularis. *Laryngoscope.* 88:12–37.
15. Komune, S., and T. Morimitsu. 1985. Dissociation of the cochlear microphonics and endocochlear potential after injection of ethacrynic acid. *Arch. Otorhinolaryngol.* 241:149–156.
16. Wang, Y., E. Fallah, and E. S. Olson. 2019. Adaptation of cochlear amplification to low endocochlear potential. *Biophys. J.* 116:1769–1786.
17. Mills, D. M., S. J. Norton, and E. W. Rubel. 1993. Vulnerability and adaptation of distortion product otoacoustic emissions to endocochlear potential variation. *J. Acoust. Soc. Am.* 94:2108–2122.
18. Schmiedt, R. A., H. Lang, …, B. A. Schulte. 2002. Effects of furosemide applied chronically to the round window: a model of metabolic presbyacusis. *J. Neurosci.* 22:9643–9650.
19. Fridberger, A., J. B. de Monvel, …, A. Nuttall. 2004. Organ of Corti potentials and the motion of the basilar membrane. *J. Neurosci.* 24:10057–10063.
20. Dong, W., and E. S. Olson. 2013. Detection of cochlear amplification and its activation. *Biophys. J.* 105:1067–1078.
21. Fallah, E., C. E. Strimbu, and E. S. Olson. 2019. Nonlinearity and amplification in cochlear responses to single and multi-tone stimuli. *Hear. Res.* 377:271–281.
22. Dallos, P., and M. A. Cheatham. 1976. Production of cochlear potentials by inner and outer hair cells. *J. Acoust. Soc. Am.* 60:510–512.
23. Sirjani, D. B., A. N. Salt, …, S. A. Hale. 2004. The influence of transducer operating point on distortion generation in the cochlea. *J. Acoust. Soc. Am.* 115:1219–1229.
24. Vavakou, A., N. P. Cooper, and M. van der Heijden. 2019. The frequency limit of outer hair cell motility measured in vivo. *elife.* 8:e47667.
25. Pappa, A. K., K. A. Hutson, …, D. C. Fitzpatrick. 2019. Hair cell and neural contributions to the cochlear summating potential. *J. Neurophys.* 121:2163–2180.
26. Nordmann, A. S., B. A. Bohne, and G. W. Harding. 2000. Histopathological differences between temporary and permanent threshold shift. *Hear. Res.* 139:13–30.
27. Vélez-Ortega, A. C., M. J. Freeman, …, G. I. Frolenkov. 2017. Mechanotransduction current is essential for stability of the transducing stereocilia in mammalian auditory hair cells. *eLife.* 6:e24661.
28. Lin, N. C., C. E. Strimbu, …, E. S. Olson. 2018. Adapting a commercial spectral domain optical coherence tomography system for time-locked displacement and physiological measurements. *AIP Conf. Proc.* 1965:080004.
29. Cooper, N. P., A. Vavakou, and M. van der Heijden. 2018. Vibration hotspots reveal longitudinal funneling of sound-evoked motion in the mammalian cochlea. *Nat. Commun.* 9:3054.
30. Versteegh, C. P., and M. van der Heijden. 2012. Basilar membrane responses to tones and tone complexes: nonlinear effects of stimulus intensity. *J. Assoc. Res. Otolaryngol.* 13:785–798.
31. Chen, F., D. Zha, …, A. L. Nuttall. 2011. A differentially amplified motion in the ear for near-threshold sound detection. *Nat. Neurosci.* 14:770–774.
32. Lee, H. Y., P. D. Raphael, …, J. S. Oghalai. 2016. Two-dimensional cochlear micromechanics measured in vivo demonstrate radial tuning within the mouse organ of corti. *J. Neurosci.* 36:8160–8173.
33. Ren, T., W. He, and D. Kemp. 2016. Reticular lamina and basilar membrane vibrations in living mouse cochleae. *Proc. Natl. Acad. Sci. USA.* 113:9910–9915.
34. Lin, N. C., C. P. Hendon, and E. S. Olson. 2017. Signal competition in optical coherence tomography and its relevance for cochlear vibrometry. *J. Acoust. Soc. Am.* 141:395–405.
35. Jacob, S., M. Pienkowski, and A. Fridberger. 2011. The endocochlear potential alters cochlear micromechanics. *Biophys. J.* 100:2586–2594.
36. van der Heijden, M. 2005. Cochlear gain control. *J. Acoust. Soc. Am.* 117:1223–1233.

37. Dallos, P., X. Wu, …, J. Zuo. 2008. Prestin-based outer hair cell motility is necessary for mammalian cochlear amplification. *Neuron.* 58:333–339.
38. Beurg, M., J.-H. Nam, …, R. Fettiplace. 2010. Calcium balance and mechanotransduction in rat cochlear hair cells. *J. Neurophysiol.* 104:18–34.
39. Peng, A. W., T. Effertz, and A. J. Ricci. 2013. Adaptation of mammalian auditory hair cell mechanotransduction is independent of calcium entry. *Neuron.* 80:960–972.
40. Corns, L. F., S. L. Johnson, …, W. Marcotti. 2014. Calcium entry into stereocilia drives adaptation of the mechanoelectrical transducer current of mammalian cochlear hair cells. *Proc. Natl. Acad. Sci. USA.* 111:14918–14923.
41. Caprara, G. A., A. A. Mecca, …, A. W. Peng. 2019. Hair bundle stimulation mode modifies manifestations of mechanotransduction adaptation. *J. Neurosci.* 39:9098–9106.
42. Maoiléidigh, Ó. D., and A. J. Ricci. 2019. A bundle of mechanisms: inner-ear hair-cell mechanotransduction. *Trends Neurosci.* 42:221–236.
43. Rybak, L. P., and T. Morizono. 1982. Effect of furosemide upon endolymph potassium concentration. *Hear. Res.* 7:223–231.
44. Rybak, L. P., and C. Whitworth. 1986. Changes in endolymph chloride concentration following furosemide injection. *Hear. Res.* 24:133–136.
45. Sellick, P. M., and B. M. Johnstone. 1974. Differential effects of ouabain and ethacrynic acid on the labyrinthine potentials. *Pflugers Arch.* 352:339–350.
46. Ikeda, K., J. Kusakari, …, Y. Saito. 1987. The Ca2+ activity of cochlear endolymph of the Guinea pig and the effect of inhibitors. *Hear. Res.* 26:117–125.
47. Santos-Sacchi, J., L. Song, …, A. L. Nuttall. 2006. Control of mammalian cochlear amplification by chloride anions. *J. Neurosci.* 26:3992–3998.
48. Freeman, D. M., K. Masaki, …, T. F. Weiss. 2003. Static material properties of the tectorial membrane: a summary. *Hear. Res.* 180:11–27.
49. Lemons, C., J. B. Sellon, …, J. Meaud. 2019. Anisotropic material properties of wild-type and tectb $^{-/-}$ tectorial membranes. *Biophys. J.* 116:573–585.
50. Edge, R. M., B. N. Evans, …, P. Dallos. 1998. Morphology of the unfixed cochlea. *Hear. Res.* 124:1–16.
51. Allen, J. B. 1980. Cochlear micromechanics–a physical model of transduction. *J. Acoust. Soc. Am.* 68:1660–1670.
52. Zwislocki, J. J. 1986. Analysis of cochlear mechanics. *Hear. Res.* 22:155–169.
53. Nankali, A., Y. Wang, …, K. Grosh. 2020. A role for tectorial membrane resonance in activating the cochlear amplifier. *Scientific Reports.* 10:17620.
54. Lamb, J. S., and R. S. Chadwick. 2011. Dual traveling waves in an inner ear model with two degrees of freedom. *Phys. Rev. Lett.* 107:088101.
55. Ghaffari, R., A. J. Aranyosi, and D. M. Freeman. 2007. Longitudinally propagating traveling waves of the mammalian tectorial membrane. *Proc. Natl. Acad. Sci. USA.* 104:16510–16515.
56. Russell, I. J., P. K. Legan, …, G. P. Richardson. 2007. Sharpened cochlear tuning in a mouse with a genetically modified tectorial membrane. *Nat. Neurosci.* 10:215–223.
57. Strimbu, C. E., S. Prasad, …, A. Fridberger. 2019. Control of hearing sensitivity by tectorial membrane calcium. *Proc. Natl. Acad. Sci. USA.* 116:5756–5764.
58. Videhult Pierre, P., J. E. Rasmussen, …, G. Laurell. 2020. High-dose furosemide enhances the magnetic resonance signal of systemic gadolinium in the mammalian cochlea. *Otol. Neurotol.* 41:545–553.
59. Ding, D., H. Liu, …, R. Salvi. 2016. Ototoxic effects and mechanisms of loop diuretics. *J. Otol.* 11:145–156.
60. Santos-Sacchi, J., M. Wu, and S. Kakehata. 2001. Furosemide alters nonlinear capacitance in isolated outer hair cells. *Hear. Res.* 159:69–73.
61. Bach, D., C. Vinkler, …, S. R. Caplan. 1988. Interaction of furosemide with lipid membranes. *J. Membr. Biol.* 101:103–111.
62. Peng, A. W., R. Gnanasambandam, …, A. J. Ricci. 2016. Adaptation independent modulation of auditory hair cell mechanotransduction channel open probability implicates a role for the lipid bilayer. *J. Neurosci.* 36:2945–2956.
63. Gianoli, F., T. Risler, and A. S. Kozlov. 2017. Lipid bilayer mediates ion-channel cooperativity in a model of hair-cell mechanotransduction. *Proc. Natl. Acad. Sci. USA.* 114:E11010–E11019.
64. Rybak, L. P., T. P. Green, …, B. L. Mirkin. 1979. Elimination kinetics of furosemide in perilymph and serum of the chinchilla. Neuropharmacologic correlates. *Acta Otolaryngol.* 88:382–387.
65. Hara, A., K. Machiki, …, J. Kusakari. 1993. Pharmacokinetics of furosemide in endolymph. *Auris Nasus Larynx.* 20:247–254.